Towards constrained grid-forming control

Dominic Groß and Xue Lyu

***Abstract*—Grid-forming converters are commonly envisioned to replace conventional synchronous generators as the cornerstone of future power systems. However, compared to synchronous generators, power converters and their power sources (e.g., renewable generation, energy storage) are subject to significant physical constraints (e.g., current limits, modulation limits). Grid-forming controls are commonly designed neglecting these constraints and subsequently augmented with limiters for a subset of constraints. In this work, we propose a systematic approach to constrained grid-forming control of two-level voltage source converters interfacing photovoltaics. We first formulate grid-forming control objectives and constraints of voltage source converters and photovoltaics in a one-step optimal grid-forming control problem. Next, we leverage primal-dual dynamics to obtain a dynamic feedback controller that approximates the solution of the one-step optimal grid-forming control problem. Finally, electromagnetic transient simulations are used to illustrate the results.**

I. Introduction

Replacing conventional fuel-based synchronous generators with converter-interfaced resources results in significantly different power system dynamics and challenges standard operating paradigms and controls. In this context, grid-forming converters are commonly envisioned to replace synchronous machines as the cornerstone of future power systems. However, compared to synchronous generators, power electronic converters and their renewable generation sources have significantly different dynamics, limited inherent energy storage, and limited overcurrent and overload capability.

Grid-connected power electronics deployed today largely rely on so-called grid-following control that can provide grid-support functions but requires a stable and slowly changing ac voltage (i.e., frequency and magnitude) at the point of connection. In particular, common grid-following controls regulate their current injection relative to the voltage at the point of connection [1] and may cease operation during significant disturbances or when converter limits are reached [2]. This lack of resilient grid-support functions results in larger and more frequent frequency deviations, and jeopardizes the stability of today's power system [3], [4]. In contrast, grid-forming converters impose self-synchronizing and stable ac voltage dynamics (i.e., frequency and magnitude) at their point of connection and are widely envisioned to replace synchronous generators as the cornerstone of future power systems [3]. Prevalent grid-forming control methods include droop control [5], virtual synchronous machine control [6], and dispatchable virtual oscillator control [7]. While grid-forming controls can, in principle replace the resilient grid-support functions of synchronous generators, they have very limited overcurrent and overload capability [8], [9]. As a consequence, device constraints such as current limits [9], modulation limits, and power source limits [10] are a major concern.

Crucially, the converter current limits are often neglected in the design and analysis of grid-forming control strategies. Few works explicitly or implicitly account for select constraints such as power limits [11, Fig. 8], dc voltage limits [11, Fig. 9], or current limits [12]–[15]. However, to the best of the authors' knowledge no systematic design procedure for grid-forming controls that explicitly accounts for all relevant constraints.

The vast majority of works on grid-forming controls under converter constraints focus on current limits. The most prevalent current limiting method relies on cascaded voltage and current control and limiting of internal reference currents. This method is prone to loss of synchronization and various synchronous instability mechanisms [16]. To overcome this challenge grid-forming controls are often augmented with threshold virtual impedance current limiting [12]–[15]. However, threshold virtual impedance current limiting may result in transient overcurrent and challenging tradeoffs between transient stability and current limiting performance [14].

In contrast, in this work, we take a more fundamental view and aim to explicitly account for a wide range of constraints of grid-connected voltage source converters in the design of grid-forming control architectures. Specifically, we formulate a one-step optimal grid-forming control problem for a single-stage photovoltaic system that explicitly accounts for both system-level (e.g., frequency stabilization) and device-level (e.g., stabilizing dc voltage) objectives as well as device-level constraints (e.g., dc voltage and current limits). Our main contribution is to leverage so-called primal-dual gradient dynamics to develop a dynamic feedback controller that only requires local measurements and asymptotically tracks the optimal solution of the one-step optimal grid-forming control problem. The resulting grid-forming controller admits a straightforward interpretation. If no constraints are active, the control reduces to universal dual-port grid-forming control [17]. In addition, if a constraint is violated proportional-integral controls are activated that aim to rapidly steer the grid-forming voltage reference to a voltage that satisfies the constraints. For instance, this control contains the dc voltage limiter [11, Fig. 9]. The control performance is illustrated using electromagnetic transient simulations of an IEEE 9-bus system with a synchronous generator, a voltage source converter using dual-port grid-forming control interfacing a controllable dc source, and a single-stage photovoltaic system using the proposed constrained grid-forming control.

This work was supported in part by the National Science Foundation under Grant No. 2143188. X. Lyu is with the Pacific Northwest National Laboratory. This work was conducted while X. Lyu was with the Department of Electrical and Computer Engineering at the University of Wisconsin-Madison University. D. Groß is with the Department of Electrical and Computer Engineering at the University of Wisconsin-Madison, USA; e-mail: dominic.gross@wisc.edu

II. Review of Grid-forming Control Architectures

To motivate the control architecture developed in this work, we first briefly review the typical grid-forming control architectures for two-level voltage source converters. The most widely used architecture is the so-called dual-loop grid-forming control shown in Fig. 1. This architecture contains an outer grid-forming control that synthesizes an ac voltage reference that is tracked by inner ac voltage and ac current controls [1].

A. Outer grid-forming control

A wide range of grid-forming controls has been proposed in the literature. The most prevalent controls are droop control [5], virtual synchronous machine control [6], and dispatchable virtual oscillator control [7]. The grid-forming control typically contains a voltage oscillator, either in polar or two-dimensional euclidean coordinates, that generates an ac voltage waveform with slowly changing frequency and magnitude as well as a synchronizing feedback that synchronizes the voltage oscillator to the grid through feedback of the power or ac current injection. The vast majority of the literature neglects constraints in the design of grid-forming controls. Notable exceptions include grid-forming controls with power limiters [11, Fig. 8], dc voltage limiters [11, Fig. 9], and current limiters [18] in the outer grid-forming control.

B. Inner control loops

While the grid-forming voltage reference can be modulated directly by a voltage source converter [5], [11], [15], the most commonly used approach is to utilize cascaded inner proportional-integral for ac voltage and ac current as shown in Fig. 1. This architecture is commonly preferred because (i) the PI voltage control attenuates resonances of the voltage source converter's LCL output filter, (ii) in steady-state VSC terminal voltage tracks the grid-forming reference, and (iii) the VSC current can be easily limited by limiting the reference of the inner current controller.

However, this architecture also inherently limits the bandwidth of the voltage source converter [19]. Moreover, reference current limiting decouples the ac voltage modulated by the voltage source converter from the grid-forming reference. This may result in instability [16]. In addition, the inner control gain tuning strongly depends on the grid impedance [20], [21] that may not be accurately known. Finally, while controlling the voltage magnitude at the VSC terminal is desirable, imposing the grid-forming angle dynamics at the filter capacitor reduces the effective grid impedance as seen from the grid-forming dynamics and may result in instability [22].

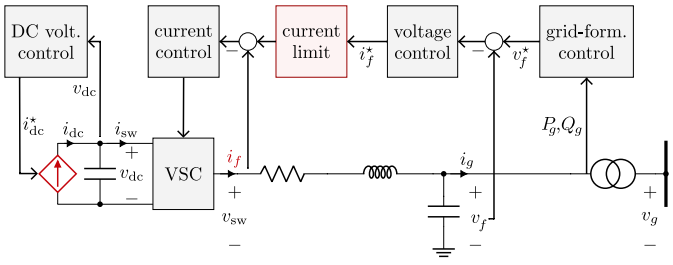

Fig. 1. Dual-loop grid-forming control architecture with cascaded inner voltage and current control.

Therefore, in this work, we will propose an alternative architecture that replaces the cascaded inner control loops with various controls that are tailored to the three aforementioned control functions (i.e., resonance damping, voltage control, current limiting).

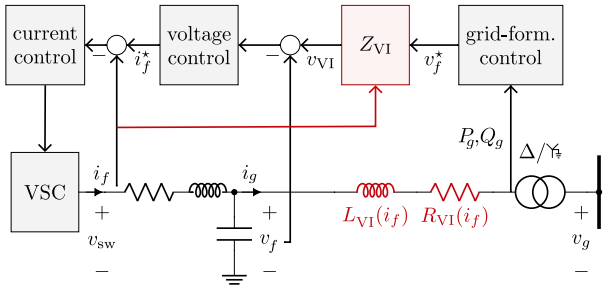

Fig. 2. Grid-forming control with threshold virtual impedance current limiting.

C. Current limiting

To protect the voltage source converter's semiconductor switches the maximum amplitude of the ac current i_{sw} needs to be limited to the maximum current capability i_{max} of the switches, i.e., $\|i_{sw}\| \leq i_{max}$. To avoid the instability associated with reference current limiting, threshold virtual resistance [12] and threshold virtual impedance [13, Sec. IV] have been proposed in the literature. These approaches emulate an increasing output resistance or impedance (see Fig. 2) if $\|i_{sw}\|$ increases beyond a threshold $i_{thr} < i_{max}$. We emphasize that threshold virtual impedance is designed with short-circuit faults in mind and may not be able to avoid overcurrent caused by phase jumps [23] or constant power loads. Moreover, inherent trade-offs exist between limiting violations of current limits, transient stability [14], and compatibility with distance protection [15].

D. Active damping

A promising alternative to replace the resonance damping functions of inner loops are active damping techniques that allow to selectively compensate harmonics beyond the timescales of grid-forming control through, e.g., virtual impedance [24], transient virtual impedance [13, Sec. II-B], virtual RC dampers [25], or derivative droop [22]. For this work, we assume that active damping controls are used to selectively compensate filter harmonics.

III. Model of Grid-forming Photovoltaics

Next, we present a reduced-order model of the single-stage PV system shown in Fig. 3. The PV current $i_{pv} : \mathbb{R}_{\geq 0} \to \mathbb{R}$ is modeled by the single-cell equivalent circuit model of a photovoltaic module

$$i_{pv}(v_{dc}) = i_{ph} + R_{sh}^{-1} v_{dc} + I_0 \left(e^{V_T^{-1} v_{dc}} - 1 \right), \qquad (1)$$

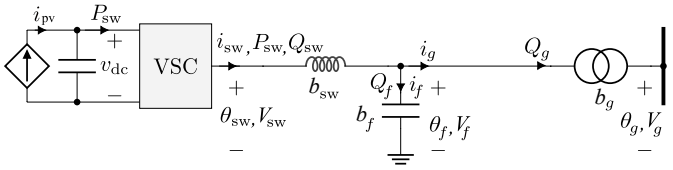

Fig. 3. Single-stage photovoltaic system with photovoltaic modules modeled as nonlinear dc current source.

where $i_{\text{ph}} \in \mathbb{R}$, $R_{\text{sh}} \in \mathbb{R}_{>0}$, $I_0 \in R_{>0}$, $V_T(t) \in R_{>0}$ denote the photogenerated current, shunt resistance, reverse saturation current, and thermal voltage, respectively. For brevity of the presentation, we assume that i_{ph} and V_T are constant. The resulting photovoltaic power generation $P_{\text{pv}} = v_{\text{dc}} i_{\text{pv}}(v_{\text{dc}}) \in \mathbb{R}$ for a typical photovoltaic module and different irradiances is shown in Fig. 4. It can be seen that a decrease of dc voltage v_{dc} results in an increase of power generation P_{pv} for $v_{\text{dc}} > v_{\text{mpp}}$ and stabilizes v_{dc}. Therefore, one aims to operate at a curtailed operating point $v_{\text{lpp}} \geq v_{\text{mpp}}$ while ensuring that $v_{\text{dc}} \geq v_{\text{mpp}}$. Moreover, current flowing into the photovoltaic module (i.e., $i_{\text{pv}} < 0$) will damage the photovoltaic module and needs to be avoided.

Next, we model the power flow across the network using the dc power flow approximation. This results in $P_{\text{sw}} = b_{\text{eq}}(\theta_{\text{sw}} - \theta_g)$ with equivalent susceptance $b_{\text{eq}} = \frac{b_{\text{sw}} b_{\text{g}}}{b_{\text{sw}} + b_{\text{g}}} \in \mathbb{R}_{>0}$ between the converter switch terminal and the (unknown) grid voltage. Moreover, the reactive power injection $Q_{\text{g}} \in \mathbb{R}$ is given by $Q_{\text{g}} = b_{\text{g}}(V_f - V_{\text{g}})$ and the magnitude $V_f(V_{\text{sw}}, V_{\text{g}}) \in \mathbb{R}_{\geq 0} \times \mathbb{R}_{\geq 0} \to \mathbb{R}_{\geq 0}$ at the filter capacitor is given by

$$V_f = \frac{b_{\text{sw}} V_{\text{sw}} + b_{\text{g}} V_{\text{g}}}{b_f + b_{\text{sw}} + b_{\text{g}}}. \tag{2}$$

For control design purposes, we consider the averaged model of a two-level VSC [26, Ch. 5.3] and assume that the LC filter and transformer are lossless. Under this assumption, the voltage phase angle $\theta_{\text{sw}}(t)$ and magnitude $V_{\text{sw}}(t)$ are the control inputs and V_{sw} is restricted to $0 \leq V_{\text{sw}}(t) \leq \frac{1}{2} v_{\text{dc}}(t)$ for all times $t \in \mathbb{R}_{>0}$. Moreover, a one-step forward prediction $v_{\text{dc}}^{+} \in \mathbb{R}_{\geq 0}$ of the dc-link voltage v_{dc} is given by

$$v_{\text{dc}}^{+}(v_{\text{dc}}, P_{\text{pv}}, P_{\text{sw}}) = v_{\text{dc}} + \frac{\tau_s}{C_{\text{dc}} v_{\text{dc}}^{\star}} (P_{\text{pv}} - P_{\text{sw}}) \tag{3}$$

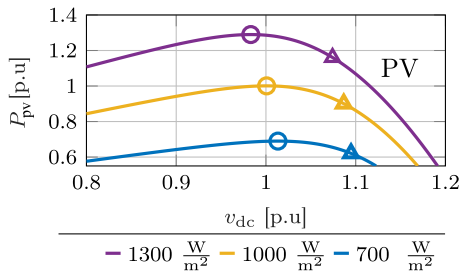

Fig. 4. Photovoltaic power generation, maximum power point v_{mpp} (circle), and limited power point v_{lpp} (triangle) for a typical photovoltaic system and different irradiances.

with controller time step $\tau_s \in \mathbb{R}_{>0}$, dc-link capacitance $C_{\text{dc}} \in \mathbb{R}_{>0}$, and nominal dc voltage $v_{\text{dc}}^{\star} \in \mathbb{R}_{>0}$. We model the converter current $i_{\text{sw}} \in \mathbb{R}^2$ in a dq frame at the nominal frequency ω_0 as $i_{\text{sw}} = \mathcal{J} \frac{b_{\text{sw}} b_{\text{g}}}{b_{\text{sw}} + b_{\text{g}} + b_f} (v_{\text{sw}} - v_g) + \mathcal{J} \frac{b_{\text{sw}} b_f}{b_{\text{sw}} + b_{\text{g}} + b_f} v_{\text{sw}}$, where $\mathcal{J} = \left[\begin{smallmatrix} 0 & -1 \\ 1 & 0 \end{smallmatrix}\right]$ denotes the 90° rotation matrix. Finally, we use $\omega_{\text{sw}}(t) = (\theta_{\text{sw}}(t) - \theta_{\text{sw}}(t-1))/\tau_s$ to denote the frequency of the ac voltage at the VSC switch terminal.

IV. Constrained GFM control of PV

A. One-step optimal GFM control

The control objective is to stabilize the single-stage PV system at an operating point $(\omega_0, v_{\text{lpp}}, V_f^{\star}, Q_{\text{g}}^{\star})$. To encode this objective, we define the vector $y(t) := (v_{\text{dc}}(t), P_{\text{pv}}(t), P_{\text{sw}}(t), Q_{\text{g}}(t), V_f(t), i_{\text{pv}}(t), i_{\text{sw}}(t), \theta_{\text{sw}}(t-1))$ of measured system outputs and previous control inputs, the control inputs $u(t) := (\theta_{\text{sw}}(t), V_{\text{sw}}(t))$, and unknown inputs $w(t) := (\theta_{\text{g}}(t), V_{\text{g}}(t))$. Then, we can formulate the cost function

$$\begin{aligned} J(y,u) :=& \tfrac{1}{2}(\omega_{\text{sw}} - \omega_0)^2 + \tfrac{m_{\text{dc}}}{2}(v_{\text{dc}}^{+} - v_{\text{lpp}})^2 + \\ & \tfrac{1}{2\tau_V}(V_f - V_f^{\star})^2 + \tfrac{m_q}{2\tau_V}(Q_{\text{g}} - Q_g^{\star})^2 \end{aligned}$$

with dc voltage droop coefficient $m_{\text{dc}} \in \mathbb{R}_{>0}$, voltage control time constant $\tau_V \in \mathbb{R}_{>0}$, and reactive power droop coefficient $m_q \in \mathbb{R}_{>0}$. Moreover, we encode the $n_c = 4$ constraints of the single-stage PV system using $g(z,y) \leq 0_{n_c}$ and

$$g(y,u) := (v_{\text{mpp}} - v_{\text{dc}}^{+}, V_{\text{sw}} - \frac{1}{2} v_{\text{dc}}, -i_{\text{pv}}, \|i_{\text{sw}}\| - i_{\max}). \tag{4}$$

This results in the one-step optimal GFM control problem

$$\min_{u(t)} J(y(t), u(t)), \text{ s.t. } g(y(t), u(t)) \leq 0. \tag{5}$$

Notably, this problem cannot be solved for $u(t)$ because some entries of $y(t)$ are functions of the unknown exogenous inputs $w(t)$ (e.g., $P_{\text{sw}}(t)$ depends on $\theta_{\text{g}}(t)$). However, for the problem at hand, $J(u,y)$ and $g(u,y)$ can be directly obtained at each point in time using local measurements. Crucially, the gradient $\nabla_u y$ can be expressed as a function of u, i.e., $\nabla_u y = \mu(u)$ is independent of w. This suggests that first-order methods can be used to construct an online algorithm that asymptotically tracks the optimal solution of (5).

B. Solution via dynamic feedback control

To formalize the previous observation and construct a dynamic feedback controller that asymptotically tracks the optimal solution of (5), we introduce the dual multipliers $\lambda \in \mathbb{R}_{\geq 0}^{n_c}$, penalty coefficient $k_{p,n} \in \mathbb{R}_{>0}^{n_c}$ and form the augmented Lagrangian

$$\mathcal{L}(y,u,\lambda) = J(y,u) + \sum_{n=1}^{n_c} \frac{k_{p,n}}{2} \max(g_n(y,u), 0)^2 + \lambda_n g_n(y,u).$$

where $g_n(y,u)$ is the n-th entry of $g(y,u)$. The optimization problem (5) can be solved by the discrete-time primal-dual gradient method

$$u(t) = u(t-1) - \nabla_u \mathcal{L}(y,u,\lambda), \tag{6a}$$

$$\lambda(t) = \max(\lambda(t-1) + K_I \nabla_\lambda \mathcal{L}(y,u,\lambda), 0) \tag{6b}$$

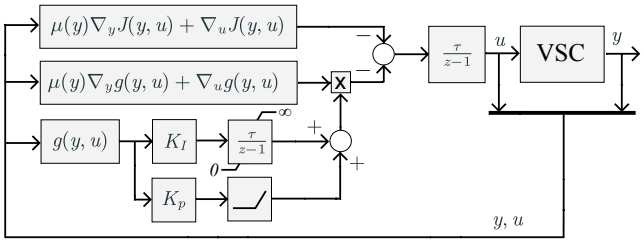

Fig. 5. Feedback controller tracking the solution of the one-step optimal control problem.

where $K_I = \text{diag}\{k_{i,n}\}_{n=1}^{n_c}$ with $k_{i,n} \in \mathbb{R}_{>0}$ is a step size for the dual update and we only perform one iteration of the primal-dual algorithm per time step. Next, we note that

$$\nabla_u \mathcal{L}(u,y,\lambda) = \mu(y)\nabla_y J(y,u) + \nabla_u J(y,u) + (K_p \max(g(y,u), 0_{n_c}) + \lambda)(\mu(y)\nabla_y g(y,u) + \nabla_u g(y,u))$$

and $\nabla_\lambda \mathcal{L}(y,u,\lambda) = g(y,u)$. The primal-dual algorithm (6) can then be interpreted as nonlinear PI control of the internal oscillator voltage $(\theta_{\text{sw}}, V_{\text{sw}})$ shown in Fig. 5. In other words, $K_p == \text{diag}\{k_{p,n}\}_{n=1}^{n_c}$ and K_I are proportional gains of nonlinear proportional-integral controls that act on $(\theta_{\text{sw}}, V_{\text{sw}})$ in response to constraint violations. We emphasize that this approach does not guarantee constraint satisfaction for all times $t \in \mathbb{R}_{>0}$. However, small and brief constraint violations are permissible in the application at hand.

C. Grid-forming response and control architecture

The overall grid-forming control architecture that results from combining (6) with suitable active damping techniques is shown in Fig. 6.

Notably, the reference voltage oscillator is now an inner control whose ac voltage, up to active damping acting on much faster time scales, is always tracked by the VSC. Several outer loops can be identified that (i) synchronize the GFM oscillator to the grid, (ii) control the filter voltage V_f, and (iii) act on the GFM oscillator voltage when constraints are violated. In particular, neglecting the constraints (i.e., $g(y,u) = 0_{n_c}$), the dynamics of $\omega_{\text{sw}}(t)$ reduce to

$$\omega_{\text{sw}}(t) = \omega_0 + k_\omega(v_{\text{dc}}(t) - v_{\text{lpp}}) + k_\theta(P_{\text{pv}}(t) - P_{\text{sw}}(t))$$

with $k_\omega := \frac{m_{\text{dc}} b_{\text{g}} b_{\text{sw}}}{C_{\text{dc}} v_{\text{dc}}^\star (b_{\text{g}} + b_{\text{sw}})}$ and $k_\theta := \frac{\tau_s}{C_{\text{dc}} v_{\text{dc}}^\star} k_\omega$. In other words, a discrete-time implementation of universal dual-port GFM control [17, Sec. IV]. Linearizing P_{pv} at v_{lpp} results in $P_{\text{pv}} - P_{\text{pv}}(v_{\text{lpp}}) = k_{\text{pv}}(v_{\text{dc}} - v_{\text{lpp}})$ and the steady-state droop

$$\omega_{\text{sw}}(t) - \omega_0 = k_\omega k_{\text{pv}}(P_{\text{pv}} - P_{\text{pv}}(v_{\text{lpp}}))$$

Moreover, neglecting the constraints (i.e., $g(y,u) = 0_{n_c}$), it can be verified that the steady-state voltage magnitude is given by

$$V_f(t) - V_f^\star = m_q(Q_{\text{g}}(t) - Q_{\text{g}}^\star), \tag{7}$$

i.e., standard $Q - V$ droop control [1, Fig. 8] imposed at the filter capacitor. Finally, noting that $\nabla_{\theta_{\text{sw}}} v_{\text{dc}}^+ = -\tau_s k_\omega$ and $\nabla_{V_{\text{sw}}} v_{\text{dc}}^+ = 0$, the feedback handling constraint $v_{\text{mpp}} - v_{\text{dc}}^+ \leq 0$ in (6) is a discrete-time implementation of the continuous time dc voltage limiter [11, Fig. 9 with $K_{dv_{\text{dc}}} = 0$].

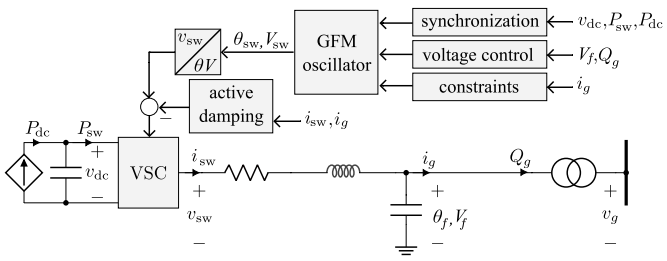

Fig. 6. Grid-forming control with grid-forming oscillator (GFM oscillator) as inner control and synchronization, voltage control, and constraint handling as outer controls.

V. Case Study

To illustrate the results electromagnetic transient simulations of the IEEE 9-bus system shown in Fig. 7 are conducted in Simscape Electrical in MATLAB/Simulink.

A. Benchmark system

The 100 MVA synchronous generator at bus 1 is modeled using an 8−th order model with exciter, automatic voltage regulator, delta-omega multiband power system stabilizer, and a first-order turbine/governor model with 5% speed droop [10, Tab. I]. The rated power of the two-level voltage source converters at bus 2 and bus 3 is 100 MVA. The voltage source converters represent an aggregate of two hundred 500 kVA low-voltage two-level voltage source converters and are modeled using average models with LC output filter, and LV/MV transformer not shown in Fig. 7. Please see [10, Tab. I] and [27, Sec. VI] for detailed parameters. The voltage source converter at bus 2 interfaces a controllable dc source (e.g., battery) and uses universal dual-port grid-forming control (see [17]). The voltage source converter at bus 3 interfaces photovoltaics and uses the constrained grid-forming control (6). Transient virtual impedance [13, Sec. II-B] is used for active damping.

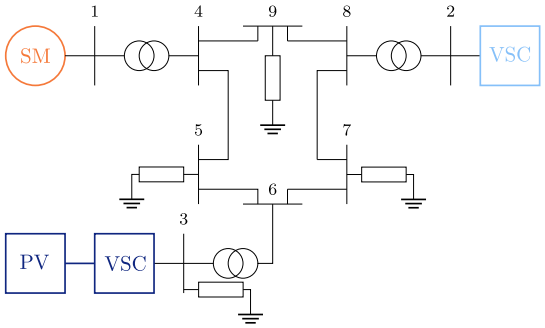

Fig. 7. IEEE 9-bus system with a synchronous generator and two grid-forming two-level voltage source converters. The voltage source converter at bus 2 interfaces a controllable dc source and uses universal dual-port grid-forming control. The voltage source converter at bus 3 interfaces PV and uses the constrained grid-forming control shown in Fig. 5.

B. High-impedance fault

First, we consider a high-impedance fault on the medium voltage side of the MV/HV transformer on bus 3. Simulation results are shown in Fig. 8.

After applying the fault at $t = 20$ s, the grid voltage reduces and the voltage V_{sw} increases to support the voltage V_f at the converter terminal. Once the ac current magnitude $\|i_{\text{sw}}\|$ increases beyond $i_{\max} = 1.2$ pu, the current limiting control activates and prevents V_{sw} from increasing further. While the current is eventually limited to $i_{\max} = 1.2$ pu, a significant transient is observed. The root cause of this transient are the quasi-steady-state circuit models presented in Sec. III. These models do not capture circuit dynamics and are used to compute control actions via (6). This inherently limits the performance and stability of the proposed control under severe disturbances such as short-circuit faults. An important area for future work is to resolve this challenge by explicitly accounting for circuit dynamics in the proposed framework. The fault is cleared at $t = 20.6$ s and the grid-forming photovoltaic system rapidly returns to the pre-fault operating point.

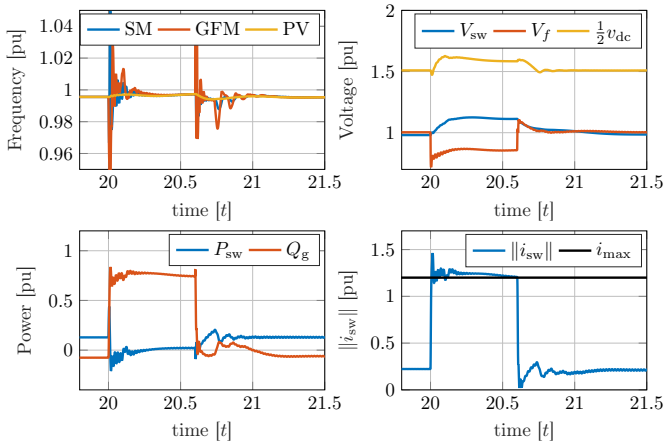

Fig. 8. Simulation results for a high impedance fault at bus 3 at $t = 20$ s. Synchronous generator (SG), grid-forming voltage source converter at bus 2 (GFM), and grid-forming photovoltaic system (PV).

C. Reactive power overload

Next, we consider an operating point with high photovoltaic module temperature (i.e., $T = 65°$) and low headroom in the modulation constraint (i.e., the pre-contingency voltage magnitude $V_{\text{sw}}(t)$ is close to $\frac{1}{2}v_{\text{lpp}}$). To drive the grid-forming photovoltaic system onto the modulation constraint $V_{\text{sw}}(t) \leq \frac{1}{2}v_{\text{dc}}$ we connect an additional 1 pu constant reactive power load at bus 3. Simulation results are shown in Fig. 9.

After connecting the load at $t = 20$ s, the voltage magnitude V_f decreases. In response,V_{sw} increases to increase the voltage V_f and realize the $Q-V$ droop (7). However, V_{sw} is limited by the modulation constraint $V_{\text{sw}} \leq \frac{1}{2}v_{\text{dc}}$. Next, due to the load dynamics, the current i_{sw} increases to the limit $i_{\max} = 1.2$ pu. At this point, one may decrease $\|i_{\text{sw}}\|$ by increasing V_{sw} or decreasing the active power injection P_{sw}. Since V_{sw} is already at the modulation limit, the control decreases P_{sw} and, after a brief negligible overshoot, limits the current to $i_{\max} = 1.2$ pu.

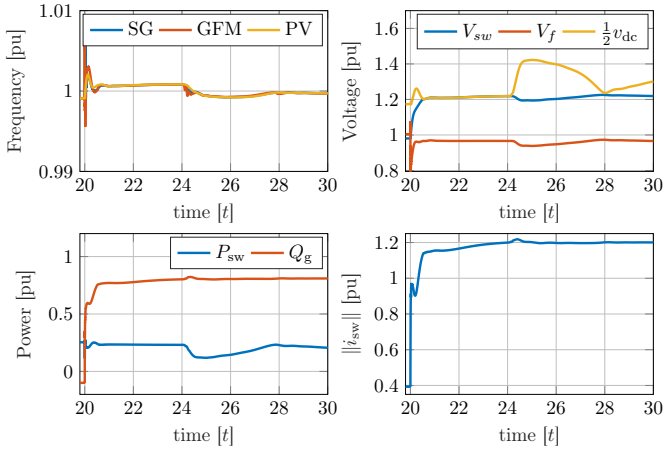

Fig. 9. Simulation results for an increase in reactive power load at $t = 20$ s. Synchronous generator (SG), grid-forming voltage source converter at bus 2 (GFM), and grid-forming photovoltaic system (PV).

D. Reverse PV current

To illustrate the control response to the constraint $i_{\text{pv}} \geq 0$, we disconnect the load shown in Fig. 7 at bus 3. Simulation results are shown in Fig. 10. In response to the load decrease at $t = 20$ s the frequency of the synchronous generator and the voltage source converter at bus 2 increases. The control for the constraint $i_{\text{pv}} \geq 0$ activates and the frequency of the photovoltaic system at bus 3 increases at a lower rate to limit the active power P_{sw} at zero.

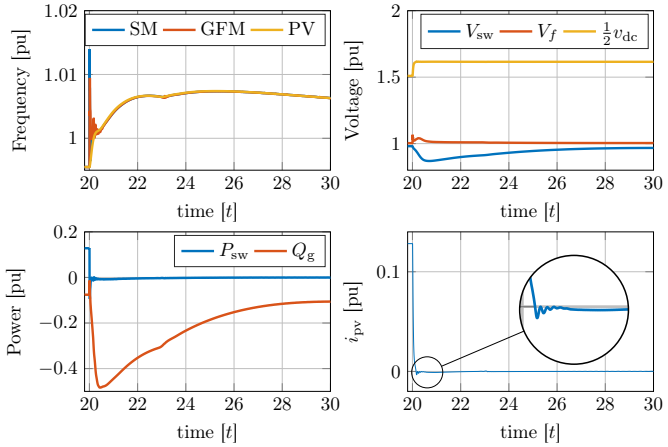

Fig. 10. Simulation results for disconnecting the load at bus 3 at $t = 20$ s. Synchronous generator (SG), grid-forming voltage source converter at bus 2 (GFM), and grid-forming photovoltaic system (PV).

E. DC voltage limit

Finally, we increase the load at bus 2 by 0.47 pu to drive the GFM PV system onto the constraint $v_{\text{dc}} \geq v_{\text{mpp}}$. Simulation results are shown in Fig. 11. Due to the load increase the frequency of the synchronous generator and two voltage source

converters drops. It can be seen that the dc current $i_{\text{sw}}^{\text{dc}}$ flowing into the voltage source converter increases beyond the photovoltaic generation i_{pv}. Consequently, v_{dc} decreases and the control for the constraint $v_{\text{dc}} \geq v_{\text{mpp}}$ activates and further reduces the grid-forming photovoltaic system frequency to reduce the active power injection P_{sw} and hence $i_{\text{sw}}^{\text{dc}}$.

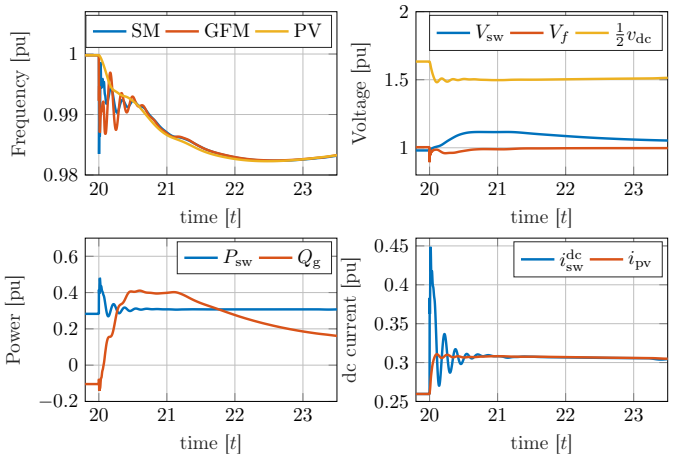

Fig. 11. Simulation results for an increase in load at $t = 20$ s. Synchronous generator (SG), VSC at bus 2 (GFM), and PV GFM (PV).

VI. Conclusion

In this paper, we developed a constrained grid-forming control for a grid-connected photovoltaic system that systematically and explicitly accounts for a wide range of constraints. Grid-forming control objectives and constraints of voltage source converters and photovoltaics are formalized in a constrained one-step optimal grid-forming control problem. Then, primal-dual dynamics are leveraged to formulate a dynamic feedback controller that asymptotically tracks the solution of the constrained one-step optimal grid-forming problem using only local measurements. In the unconstrained case, the dynamic feedback controller recovers known grid-forming controls. Finally, the control performance is illustrated using an electromagnetic transient simulation.

References

[1] J. Rocabert, A. Luna, F. Blaabjerg, and P. Rodríguez, "Control of power converters in ac microgrids," *IEEE Trans. Power Electron.*, vol. 27, no. 11, pp. 4734–4749, 2012.

[2] "1200 MW fault induced solar photovoltaic resource interruption disturbance report," NERC, Tech. Rep., 2017.

[3] F. Milano, F. Dörfler, G. Hug, D. J. Hill, and G. Verbič, "Foundations and challenges of low-inertia systems (invited paper)," in *Power Systems Computation Conference*, 2018.

[4] W. Winter, K. Elkington, G. Bareux, and J. Kostevc, "Pushing the limits: Europe's new grid: Innovative tools to combat transmission bottlenecks and reduced inertia," *IEEE Power Energy Mag.*, vol. 13, no. 1, pp. 60–74, 2015.

[5] M. Chandorkar, D. Divan, and R. Adapa, "Control of parallel connected inverters in standalone AC supply systems," *IEEE Trans. Ind. Appl.*, vol. 29, no. 1, pp. 136–143, 1993.

[6] S. D'Arco, J. A. Suul, and O. B. Fosso, "A virtual synchronous machine implementation for distributed control of power converters in smartgrids," *Electr. Pow. Sys. Res.*, vol. 122, pp. 180–197, 2015.

[7] D. Groß, M. Colombino, B. Jean-Sébastien, and F. Dörfler, "The effect of transmission-line dynamics on grid-forming dispatchable virtual oscillator control," *IEEE Trans. Control Netw. Syst.*, vol. 6, no. 3, pp. 1148–1160, 2019.

[8] J. Jia, G. Yang, and A. H. Nielsen, "A review on grid-connected converter control for short-circuit power provision under grid unbalanced faults," *IEEE Trans. Power Del.*, vol. 33, no. 2, pp. 649–661, 2018.

[9] G. Denis, T. Prevost, M.-S. Debry, F. Xavier, X. Guillaud, and A. Menze, "The Migrate project: the challenges of operating a transmission grid with only inverter-based generation. a grid-forming control improvement with transient current-limiting control," *IET Renewable Power Generation*, vol. 12, no. 5, pp. 523–529, 2018.

[10] A. Tayyebi, D. Groß, A. Anta, F. Kupzog, and F. Dörfler, "Frequency stability of synchronous machines and grid-forming power converters," *IEEE Trans. Emerg. Sel. Topics Power Electron.*, vol. 8, no. 2, pp. 1004–1018, 2020.

[11] Z. Chen, D. Pattabiraman, R. H. Lasseter, and T. M. Jahns, "CERTS microgrids with photovoltaic microsources and feeder flow control," in *IEEE Energy Conversion Congress and Exposition*, 2016.

[12] F. Salha, F. Colas, and X. Guillaud, "Virtual resistance principle for the overcurrent protection of pwm voltage source inverter," in *IEEE PES Innovative Smart Grid Technologies Conference Europe*, 2010.

[13] A. D. Paquette and D. M. Divan, "Virtual impedance current limiting for inverters in microgrids with synchronous generators," *IEEE Trans. Ind. Appl.*, vol. 51, no. 2, pp. 1630–1638, 2015.

[14] B. Fan, T. Liu, F. Zhao, H. Wu, and X. Wang, "A review of current-limiting control of grid-forming inverters under symmetrical disturbances," *IEEE Open Journal of Power Electronics*, vol. 3, pp. 955–969, 2022.

[15] N. Baeckeland, D. Venkatramanan, M. Kleemann, and S. Dhople, "Stationary-frame grid-forming inverter control architectures for unbalanced fault-current limiting," *IEEE Trans. Energy Convers.*, vol. 37, no. 4, pp. 2813–2825, 2022.

[16] H. Xin, L. Huang, L. Zhang, Z. Wang, and J. Hu, "Synchronous instability mechanism of P-f droop-controlled voltage source converter caused by current saturation," *IEEE Trans. Power Syst.*, vol. 31, no. 6, pp. 5206–5207, 2016.

[17] I. Subotić, , and D. Groß, "Universal dual-port grid-forming control: bridging the gap between grid-forming and grid-following control," 2023, arXiv:2304.04939.

[18] D. Groß and F. Dörfler, "Projected grid-forming control for current-limiting of power converters," in *Allerton Conference on Communication, Control, and Computing*, 2019, pp. 326–333.

[19] S. Bala and G. Venkataramanan, "On the choice of voltage regulators for droop-controlled voltage source converters in microgrids to ensure stability," in *IEEE Energy Conversion Congress and Exposition*, 2010, pp. 3448–3455.

[20] T. Qoria, F. Gruson, F. Colas, X. Guillaud, M. Debry, and T. Prevost, "Tuning of cascaded controllers for robust grid-forming voltage source converter," in *Power Systems Computation Conference*, 2018.

[21] I. Subotič, D. Groß, M. Colombino, and F. Dörfler, "A Lyapunov framework for nested dynamical systems on multiple time scales with application to converter-based power systems," *IEEE Trans. Autom. Control*, vol. 66, no. 12, pp. 5909–5924, 2021.

[22] D. Groß, "Compensating network dynamics in grid-forming control," in *Allerton Conference on Communication, Control, and Computation*, 2022.

[23] Z. Zeng, P. Bhagwat, M. Saeedifard, and D. Groß, "Hybrid threshold virtual impedance for fault current limiting in grid-forming converters," in *IEEE Energy Conversion Congress and Exposition*, 2023.

[24] J. He and Y. W. Li, "Analysis, design, and implementation of virtual impedance for power electronics interfaced distributed generation," *IEEE Trans. Ind. Appl.*, vol. 47, no. 6, pp. 2525–2538, 2011.

[25] X. Wang, F. Blaabjerg, and P. C. Loh, "Virtual RC damping of LCL-filtered voltage source converters with extended selective harmonic compensation," *IEEE Trans. Power Electron.*, vol. 30, no. 9, pp. 4726–4737, 2015.

[26] A. Yazdani and R. Iravani, *Voltage-Sourced Converters in Power Systems: Modeling, Control, and Applications*. Wiley, 2010.

[27] I. Subotić and D. Groß, "Power-balancing dual-port grid-forming power converter control for renewable integration and hybrid AC/DC power systems," *IEEE Trans. Control Netw. Syst.*, vol. 9, no. 4, pp. 1949–1961, 2022.